Published in final edited form as:
ChemMedChem. 2014 June ; 9(6): 1238–1243. doi:10.1002/cmdc.201400014.

SpiroZin1: A Reversible and pH-Insensitive, Reaction-based, Red-fluorescent Probe for Imaging Biological Mobile Zinc

Dr. Pablo Rivera-Fuentes[a] and **Prof. Stephen J. Lippard**[a]

Stephen J. Lippard: lippard@mit.edu

[a]Department of Chemistry, Massachusetts Institute of Technology, Cambridge, MA 02139, USA Fax: +1-617-258-8150, Homepage: http://web.mit.edu/lippardlab/

Abstract

A reversible, reaction-based sensor for biological mobile zinc was designed, prepared, and characterized. The sensing mechanism of this probe is based on the zinc-induced, ring-opening reaction of spirobenzopyran to give a cyanine fluorophore that emits in the deep-red region of the electromagnetic spectrum. This probe is not activated by protons and operates efficiently in aqueous solution at pH 7 and high ionic strength. The mechanism of this reaction was studied by using a combination of kinetics experiments and DFT calculations. The biocompatibility of the probe was demonstrated in live HeLa cells.

Keywords

Bioinorganic chemistry; Biosensors; Coordination chemistry; Spirobenzopyran

Introduction

Zinc is an essential trace element in biology.[1, 2] Although most biological zinc occurs as a structural component of proteins,[3] there are pools of readily chelatable, or mobile, zinc in specific organs such as the brain,[4, 5] pancreas,[6] and prostate.[7] In the hippocampus, high concentrations of mobile zinc stored in vesicles at glutamatergic synapses[8] have been conclusively associated with long-term potentiation.[9] Mobile zinc also plays an important role in sensory perception.[10–13] In the pancreas, insulin crystallization depends on the expression of the zinc transporter ZnT8,[14] and zinc can be used as a surrogate for imaging insulin secretion.[15] Mobile zinc accumulates in epithelial cells in the prostate,[16] and a firm link has been established between intracellular zinc levels and prostate cancer.[17]

The development of luminescent sensors for mobile zinc has provided important tools for investigating its many biological roles.[18, 19] Although these probes utilize various sensing mechanisms, most rely on the modulation of photoinduced electron transfer (PET) for their fluorescence turn-on response.[20] PET-based probes are often sensitive to pH, however,[21, 22] and do not operate efficiently at long wavelengths, >700 nm. These

Correspondence to: Stephen J. Lippard, lippard@mit.edu.

Supporting information for this article is available on the WWW under http://dx.doi.org/XX

limitations restrict the information that can be obtained using fluorescent sensors, especially because long wavelength emitting probes are preferred for studies in vivo.[23, 24]

Probes that emit a luminescent signal following a chemical reaction have been developed recently.[25, 26] A limitation of such “reaction-based” probes, however, is their irreversibility, which precludes their application to real-time monitoring of concentration changes.

In the present study, we sought to prepare a reaction-based sensor for Zn^{2+} that is reversible, pH-insensitive, and emits at long wavelengths. We recognized that switching reactions offer an ideal platform for sensor development because of their reversibility. The equilibrium between spirobenzopyrans and their cyanine forms provides an excellent example of a thermodynamically reversible switching reaction that has been exploited extensively in materials science.[27] This reaction is generally driven by light, but examples of chelation-induced switching have also been reported.[28, 29] Here, we report the design, synthesis, and mechanistic study of SpiroZin1, a sensor that comprises dipicolylamine as the zinc-binding unit, appended to a spirobenzopyran scaffold as well as its application in live cell imaging.

Results and Discussion

Synthesis and Characterization

SpiroZin1 was synthesized in a one-pot procedure starting from commercially available dipicolylamine (DPA) and the readily accessible building blocks **1** and **2** (Scheme 1A). The reaction involves nucleophilic attack of DPA on the benzylic chlorine of **2**, followed by Knoevenagel condensation of the intermediate aldehyde with **1**. SpiroZin1 was isolated as a pale pink, waxy solid that forms nearly colorless solutions in common organic solvents such as CH_3OH, CH_3CN, CH_2Cl_2, and DMSO. ^1H NMR spectroscopic measurements in CD_3OD (Figures SI-1 and SI-2) revealed two diastereotopic singlets for the two methyl groups on the dihydroindole ring and two diastereotopic doublets for the methylene that connects the DPA arm (Scheme 1B) with the spirobenzopyran core (Figure SI-3). In addition, the two vinylic hydrogen atoms on the benzopyran ring have a coupling constant $^3J_{H–H}$ = 7.5 Hz, consistent with cis stereochemistry. These observations demonstrate that SpiroZin1 exists predominantly as the spirobenzopyran isomer (Scheme 1B). Addition of 1 equiv. of $ZnCl_2$ turned the color of SpiroZin1 to a deep red. ^1H NMR spectra of this solution revealed only one singlet for the methyl groups on the indolenine ring and a singlet for the methylene group that connects DPA with the rest of the molecule (Scheme 1B). The coupling constant of the vinylic hydrogens also changed to $^3J_{H–H}$ = 16.5 Hz, consistent with trans geometry of the alkene. These NMR signals prove that, in the presence of Zn^{2+}, the spirobenzopyran ring is opened to produce the cyanine form.

Sensing Properties

The photophysical properties of SpiroZin1 were investigated in aqueous buffer (50 mM PIPES, 100 mM KCl, pH 7). Under these conditions, SpiroZin1 absorbs only weakly in the region between 400–700 nm (Figure 1). No fluorescence could be detected for this solution upon excitation at 500 nm. Following addition of 10 equiv. of $ZnCl_2$, however, a strong band appeared at λ_{max} = 508 nm (1.40(3) × 10^4 M^{-1} cm^{-1}). Excitation at 508 nm produced

fluorescence in the deep-red region at λ_{max} = 650 nm (ϕ = 0.0042(7), Figure 1). Despite the low quantum yield of the probe in the zinc-bound form, SpiroZin1 efficiently detects mobile Zn^{2+} because of the very low background in both the absorption and emission spectra of the apo form.

Titration of SpiroZin1 with $ZnCl_2$ revealed formation of a 1:1 complex (Figure SI-5). We propose a binding mode involving the three nitrogen atoms of the DPA arm and the oxygen atom on the cresol ring, which triggers the spirobenzopyran ring-opening reaction. This binding mode maintains the [N_3O] coordination sphere of previously reported sensors, such as those in the ZP family,[30, 31] ZPP1,[32] and the recently reported ZBR probes.[33] SpiroZin1 chelates Zn^{2+} tightly with an apparent dissociation constant (K_d) of 21(1) pM (Figure SI-6).

The selectivity of SpiroZin1 for biologically relevant metal cations was investigated. Alkaline and alkali-earth metals produce no change in the fluorescence or absorbance spectra of SpiroZin1 (Figure SI-7). Paramagnetic transition metals increased the absorbance but not the fluorescence, suggesting that they cause ring opening, but their partially filled d-orbitals quench the fluorescence of the resulting cyanine. Cadmium increases both fluorescence and the absorbance, but to a lesser extent than zinc (Figure SI-7).

An advantage of SpiroZin1 is its ability to operate at low pH. The fluorescence of SpiroZin1 turns on at pH 4, 5, and 6 (Figure 2), but this increase is very small compared with the turn-on induced by Zn^{2+} at these pH values (Figure 2).

Mechanistic Studies

SpiroZin1 is unique among reaction-based probes because of its reversibility. We investigated the reaction kinetics of both the turn-on event induced by Zn^{2+} and the turn-off process caused by its removal following addition of the chelating agent ethylenediaminetetraacetic acid (EDTA). The turn-on process is very rapid and was monitored by stopped-flow spectrophotometry. Similar results were obtained by stopped-flow fluorescence spectroscopy (Figure SI-8). This study revealed that turn-on occurs in two steps, each of which could be modeled by a single exponential function (Figure 3). The first process is fast with $t_{1/2}$ = 5.89(9) ms and the second step is slower, with $t_{1/2}$ = 1.17(2) s. Overall, the turn-on event occurs within seconds under physiological conditions. The turn-off process, on the other hand, can be modeled by a single exponential decay as determined by fluorescence spectroscopy (Figure 3) and is slow, with $t_{1/2}$ = 8.55(1) min.

To understand the mechanism of the sensing reaction of SpiroZin1, we carried out an intrinsic reaction coordinate analysis using density functional theory (DFT) at the BP86/TZVP/LANL2DZ level of theory. We decided to model only the electronic ground state of each reaction intermediate because the experimental observations demonstrate chelation of Zn^{2+} to be the main driving force of the reaction. We note that the presence of light might influence the reaction mechanism and that our calculations are meant to provide only a qualitative representation.

The reaction was modeled starting from a zinc complex of SpiroZin1 in the spirobenzopyran form (Figure 4, structure A). The first step in the reaction is ring opening (B) to afford a cis cyanine as an intermediate (C). The calculated activation energy for this process is only 2.8 kcal mol^{-1}, which agrees qualitatively with the fast step observed by stopped-flow kinetics. The second step of the reaction is isomerization of the alkene (D) to give the final trans cyanine (E). The higher calculated activation energy of this process is also consistent with the slower kinetics measured. In the opposite direction, the slow cis/trans isomerization occurs first and is the rate-determining step, which agrees with the single exponential decay of fluorescence observed experimentally.

Live Cell Imaging

The ability of SpiroZin1 to report on the arrival of mobile zinc in live cells was assessed by using human cervical cancer cells (HeLa). HeLa cells were incubated at 37 °C with 5 μM SpiroZin1 for 30 min before imaging. Considerable intracellular red fluorescence was detected under these conditions (Figure 5, panel B). The reason for this high background fluorescence might be the relatively high concentration of endogenous mobile Zn^{2+} in HeLa cells (~100 pM)[34] and the high Zn^{2+} affinity of SpiroZin1 (21(1) pM). The intracellular fluorescence, however, increased further upon incubation of the cells with 20 μM $ZnCl_2$ and 50 μM concentrations of the Zn^{2+} ionophore 2-mercaptopyridine oxide (pyrithione) (Figure 5, panel C). Quantification of the fluorescence intensity revealed that addition of the exogenous zinc elicited a 2.5(5)-fold turn-on. Addition of the cell-permeable chelator *N*,*N*,*N*′,*N*′-tetrakis(2-pyridylmethyl)ethylenediamine (TPEN) reduced the fluorescence confirming that the fluorescence turn-on is induced by zinc (Figure 5, panel D).

Summary and Conclusions

We describe the design, synthesis, and characterization of a red-emitting sensor for mobile zinc. This sensor, SpiroZin1, is based on the ring-opening reaction of spirobenzopyran to form a fluorescent cyanine. This reaction is induced by Zn^{2+}, can be reversed upon treatment with a chelator, and operates even at low pH. Studies using stopped-flow kinetics, fluorescence spectroscopy, and DFT calculations provided mechanistic details of the sensing mechanism. The biocompatibility of this sensor was assessed in cultured HeLa cells.

The modular synthesis of SpiroZin1 allows for modification of the metal-binding site, which will be useful for tuning its affinity and selectivity. We envision that this design principle will inform the construction of probes that emit at even longer wavelengths.

Experimental Section

General Materials and Methods

All reagents were purchased from commercial sources and used as received. Compounds **1**[35] and **2**[36] were prepared according to published methods. Solvents were purified and degassed by standard procedures. NMR spectra were acquired on a Varian Inova-300 instrument. ^{1}H NMR chemical shifts are reported in ppm relative to $SiMe_4$ (δ = 0) and were referenced internally with respect to residual protons in the solvent (δ = 3.31 for (CH_3OH). Coupling constants are reported in Hz. ^{13}C NMR chemical shifts are reported in ppm

relative to $SiMe_4$ (δ = 0) and were referenced internally with respect to solvent signal (δ = 49.00 for (CD_3OD). Low-resolution mass spectra (LRMS) were acquired on an Agilent 1100 Series LC/MSD Trap spectrometer (LCMS), using electrospray ionization (ESI). High-resolution mass spectrometry (HR-ESI-MS) was conducted by staff at the MIT Department of Chemistry Instrumentation Facility on a Bruker Daltonics APEXIV 4.7 T FT-ICR-MS instrument. The IUPAC name of SpiroZin1 is provided and was determined using CS ChemBioDrawUltra 12.0.

Synthesis of 1-(pyridin-2-yl)-*N*-(pyridin-2-ylmethyl)-*N*-((1′,3′,3′,6-tetramethylspiro [chromene-2,2′-indolin]-8-yl)methyl)methanamine (SpiroZin1)—Compound **2** (150 mg, 0.728 mmol) and K_2CO_3 (302 mg, 2.18 mmol) were added to a Schlenk flask that was evacuated and refilled with nitrogen three times. A solution of DPA (290 mg, 1.46 mmol) in ethanol (7 mL) was added via syringe. The mixture was stirred at 25 °C for 1 h. Compound **1** (219 mg, 0.728 mmol) was added in one portion and the mixture was heated to reflux for 1 h. The suspension was filtered and the filtrate was evaporated. The residue was purified by flash column chromatography (Brockmann 1, basic Al_2O_3; CH_2Cl_2) to give a pale pink solid (148 mg, 40%). M.p.: 50–51 °C; R_f = 0.24 (Brockmann 1, basic Al_2O_3; CH_2Cl_2); ^{1}H NMR (300 MHz, CD_3OD): 1.13 (s, 3H), 1.24 (s, 3H), 2.20 (s, 3H), 2.66 (s, 3H), 3.33 (d, *J* = 18 Hz, 1H), 3.52 (d, *J* = 18 Hz, 1H), 3.59 (s, 4H), 5.71 (d, *J* = 7.5 Hz, 1H), 6.47 (d, *J* = 7.5 Hz, 1H), 6.75–6.87 (m, 2H), 6.81 (s, 1H), 6.99 (s, 1H), 7.00–7.10 (m, 2H), 7.18–7.23 (m, 2H), 7.45 (d, *J* = 6 Hz, 2H), 7.67–7.70 (m, 2H), 8.34 (d, *J* = 6 Hz, 2H); ^{13}C NMR (75 MHz; CD_3OD): 19.43, 19.56, 25.23, 28.06,51.30, 52.03, 59.72, 104.43, 106.60, 118.99, 119.01, 121.24, 122.46, 123.31, 123.39, 126.47, 127.40, 128.93, 129.68, 131.24, 136.88, 137.46, 148.00, 148.24, 150.38, 159.28; HR-ESI-MS: Calcd for $[C_{33}H_{35}N_4O]^+$: 503.2811, found: 503.2818.

Spectroscopic Methods

All aqueous solutions were prepared using de-ionized water with resistivity 18.2 mΩ cm^{-1}, obtained using a Milli-Q water purification system. Solvents were procured from Aldrich and used as received. Piperazine-*N*,*N*′-bis(2-ethanesulfonic acid) (PIPES) and 99.999% KCl were purchased from Calbiochem. Stock solutions of SpiroZin1 in DMSO were prepared at a concentration of 5 mM and stored at −20 °C in 1 mL aliquots and thawed immediately before each experiment. All spectroscopic measurements were conducted in aqueous buffer containing 50 mM PIPES (pH 7) and 100 mM KCl. UV-visible spectra were acquired on a Cary 50 spectrometer using quartz cuvettes from Starna (1 cm path length). Fluorescence spectra were acquired on a Photon Technology International fluorimeter. All measurements were conducted at 25 °C maintained by circulating water baths. Extinction coefficients were determined in the 1 to 5 μM range in aqueous buffer. Fluorescence quantum yields were determined by using 1 to 5 μM sensor aqueous buffer solutions, exciting at 508 nm. Fluorescence emission spectra were integrated from 550 to 800 nm. The quantum yield calculation was standardized to resorufin, with a reported quantum yield of 0.74 at pH 9.5, λ_{ex} = 572 nm.[37]

pH Titration, Metal Selectivity, and Dissociation Constant

Buffered solutions at pH 3, 4, 5, 6, and 7 were prepared by mixing different volumes of 0.1 M citric acid and 0.2 M Na_2HPO_4 in water (Table SI-1) and the pH was verified using a Mettler Toledo FE20 pH meter. The fluorescence of 5 μM SpiroZin1 in these buffered solutions was measured before and after addition of 10 equiv. of $ZnCl_2$ and the intensities were normalized with respect to 5 μM SpiroZin1 at pH 7 before addition of $ZnCl_2$.

To determine the metal selectivity of SpiroZin1, PIPES-buffered solutions (pH 7) containing 5 μM SpiroZin1 were prepared. To each solution, 100 equiv. of NaCl, $MgCl_2$, $CaCl_2$, $CdCl_2$, $NiCl_2$, $CuCl_2$, $MnCl_2$, or $CoCl_2$ were added and the fluorescence intensity measured. Cu^+ was added as a solution of $[Cu(CH_3CN)_4]PF_6$ in CH_3CN to 5 μM SpiroZin1 in CH_3CN under nitrogen. To the same solutions, 100 equiv. of $ZnCl_2$ were added and the fluorescence intensity recorded. In each case, the fluorescence intensity was normalized with respect to 5 μM SpiroZin1 in aqueous buffer.

To determine the apparent dissociation constant (K_d), solutions containing 1 mM 1,2-diaminohydroxypropanetetraacetic acid (DHPTA) and $ZnCl_2$ were prepared. The total concentration of Zn^{2+} was varied from 0.1 mM to 0.9 mM, to give buffered free Zn^{2+} concentrations ranging from 1.3×10^{-12} M to 1.1×10^{-10} M.[38] 5 μM SpiroZin1 was added to each of these solutions, which were then equilibrated in the dark for 24 h. The fluorescence of these solutions was measured and normalized with respect to 5 μM SpiroZin1 in the presence of 100 equiv. of $ZnCl_2$. The normalized fluorescence responses (R) were plotted against the concentration of free Zn^{2+} [Zn] and the resulting data was fit to the equation $R = B[Zn]/(K_d + [Zn])$, where B = 1. Minimization of this equation gave the values B = 1.03(1), $K_d = 2.1(1) \times 10^{-11}$ M, and $R^2 = 0.995$.

Kinetic Experiments

Zinc-induced ring opening of SpiroZin1 was monitored by stopped-flow UV-visible spectroscopy configured with a single-wavelength photomultiplier and a tungsten lamp. Stopped-flow data were obtained using a Hi-Tech Scientific SF-61 DX2 stopped-flow spectrophotometer. The optical change at 508 nm was recorded to assess formation of the cyanine isomer.

Solutions containing 5 μM SpiroZin1 and 500 μM $ZnCl_2$ were prepared in aqueous buffer (50 mM PIPES, 100 mM KCl, pH 7). The reactions were maintained at 25 °C with a circulating water bath. Data points were collected on a logarithmic time scale (0.001–10s). A dead time determination indicates that the first usable data points occur between 1 and 2 ms and the raw data was truncated accordingly. The data used for analysis are averages of six independent measurements and were fit to a double exponential function: $A = A_0 + B_1\exp[k_1 t] + B_2\exp[k_2 t]$, where A is the measured absorbance, A_0 the initial absorbance, k_1 and k_2 the rate constants of the two steps, t is time, and B_1 and B_2 are constants. Minimization of this equation gave the values $k_1 = 178(3)\ s^{-1}$, $k_2 = 0.59(1)\ s^{-1}$, $R^2 = 0.9997$.

The ring-closing process was monitored by fluorescence spectroscopy. A solution containing 5 μM SpiroZin1 and 5 μM $ZnCl_2$ was prepared and allowed to equilibrate in the dark for 1 h. The fluorescence of this solution was measured and 100 equiv. of EDTA were

added. The fluorescence intensity was measured every 30 s. Fluorescence emission spectra at each time point were integrated from 550 to 800 nm and plotted against time. The data were fit to a single exponential function: $F = F_0 + B_1\exp[k_1 t]$, where F is the integrated fluorescence, F_0 the initial integrated fluorescence, k_1 the rate constant, t is time, and B_1 a constant. Minimization of this equation gave the values $k_1 = 0.001351(1)\ s^{-1}$, $R^2 = 0.99992$

DFT Calculations

All calculations were carried out using ORCA 2.9.1[39] employing the BP86 functional, the TZVP basis set for C, N, O, and H, and the LANL2DZ basis set for Zn. The resolution of the identity (RI) approximation, with the appropriate auxiliary basis sets, was used in all calculations. Geometry optimizations were performed in solution by applying the implicit conductor-like screening model (COSMO) for water. The nature of the stationary points was characterized by harmonic vibrational analysis. All minima showed zero imaginary frequencies, whereas all transition states gave only one imaginary frequency along the reaction coordinate. Cartesian coordinates of all structures are provided in the SI.

Cell Culture and Staining Procedures

HeLa cells were cultured in Dulbecco's modified Eagle medium (DMEM; Cellgro, MediaTec, Inc.), supplemented with 10% fetal bovine serum (FBS; HyClone), 1% penicillin-streptomycin, 1% sodium pyruvate, and 1% L-glutamine. The cells were grown to 90% confluence at 37 °C with 5% CO_2 before being passed and plated onto poly-D-lysine coated plates 24 h before imaging. Cells used were at passage number 7. A confluence level of 50% was reached at imaging. The growth medium was replaced with dye-free DMEM containing 5 μM SpiroZin1 and 2 μM Hoechst 33528 nuclear stain, and the cells were incubated for 30 min. Cells were rinsed with PBS buffer (2 × 2 mL) before addition of fresh dye-free DMEM (2 mL) and mounted on the microscope.

Fluorescence Microscopy

Imaging experiments were performed using a Zeiss Axiovert 200M inverted epifluorescence microscope equipped with an EM-CCD digital camera (Hamamatsu) and a MS200 XY Piezo Z stage (Applied Scientific Instruments). The light source was an X-Cite 120 metal-halide lamp (EXFO) and the fluorescence images were obtained using an oil-immersion objective at 63× magnification. The fluorescence filters sets used are defined as blue: excitation G 365 nm, beamsplitter FT 395 nm, emission BP 445/50 nm; red: BP 550/25 nm, beamsplitter FT 570 nm, emission BP 605/70 nm. The microscope was operated using Volocity software (Perkin-Elmer).

The exposure time for acquisition of fluorescence images were kept constant for each series of images at each channel. To measure analyte-induced fluorescence changes, the cells were treated with dye-free DMEM containing 20 μM $ZnCl_2$ and 50 μM pyrithione for 10 min. To reverse the effect of zinc, the cells were exposed to dye-free DMEM containing 50 μM TPEN for 15 min. All these experiments were carried out on the stage of the microscope. Quantification of fluorescence intensity was performed using ImageJ (version 1.45, NIH). The whole cell was selected as the region of interest. The integrated fluorescence from the background region was subtracted from the cell body region.

Supplementary Material

Refer to Web version on PubMed Central for supplementary material.

Acknowledgments

This work was supported by NIH grant GM065519 from the National Institute of General Medical Sciences. Spectroscopic instrumentation in the MIT DCIF is maintained with funding from 1S10RR13886-01. P. R.-F. thanks the Swiss National Science Foundation for a postdoctoral fellowship and Dr. Patricia Marqués Gallego, Dr. Wei Lin, and Ms. Alexandria D. Liang for insightful discussions.

References

1. Vallee BL, Falchuk KH. Physiol Rev. 1993; 73:79–118. [PubMed: 8419966]
2. Kelleher SL, McCormick NH, Velasquez V, Lopez V. Adv Nutr. 2011; 2:101–111. [PubMed: 22332039]
3. Maret W. Met Ions Life Sci. 2013; 12:479–501. [PubMed: 23595681]
4. Frederickson CJ, Koh JY, Bush AI. Nat Rev Neurosci. 2005; 6:449–462. [PubMed: 15891778]
5. Takeda A, Nakamura M, Fujii H, Tamano H. Metallomics. 2013; 5:417–423. [PubMed: 23423555]
6. Taylor CG. BioMetals. 2005; 18:305–312. [PubMed: 16158221]
7. Franklin RB, Milon B, Feng P, Costello LC. Front Biosci. 2005; 10:2230–2239. [PubMed: 15970489]
8. Paoletti P, Vergnano AM, Barbour B, Casado M. Neuroscience. 2009; 158:126–136. [PubMed: 18353558]
9. Pan E, Zhang X-a, Huang Z, Krezel A, Zhao M, Tinberg CE, Lippard SJ, McNamara JO. Neuron. 2011; 71:1116–1126. [PubMed: 21943607]
10. Redenti S, Chappell RL. Vision Res. 2005; 45:3520–3525. [PubMed: 16181655]
11. Redenti S, Ripps H, Chappell RL. Exp Eye Res. 2007; 85:580–584. [PubMed: 17825289]
12. Jo SM, Won MH, Cole TB, Jensen MS, Palmiter RD, Danscher G. Brain Res. 2000; 865:227–236. [PubMed: 10821925]
13. Perez-Rosello T, Anderson CT, Schopfer FJ, Zhao Y, Gilad D, Salvatore SR, Freeman BA, Hershfinkel M, Aizenman E, Tzounopoulos T. J Neurosci. 2013; 33:9259–9272. [PubMed: 23719795]
14. Lemaire K, Ravier MA, Schraenen A, Creemers JWM, Van de Plas R, Granvik M, Van Lommel L, Waelkens E, Chimienti F, Rutter GA, Gilon P, in't Veld PA, Schuit FC. Proc Nat Acad Sci U S A. 2009; 106:14872–14877.
15. Li D, Chen S, Bellomo EA, Tarasov AI, Kaut C, Rutter GA, Li W-h. Proc Nat Acad Sci U S A. 2011; 108:21063–21068.
16. Costello LC, Franklin RB, Feng P. Mitochondrion. 2005; 5:143–153. [PubMed: 16050980]
17. Kolenko V, Teper E, Kutikov A, Uzzo R. Nat Rev Urol. 2013; 10:219–226. [PubMed: 23478540]
18. Que EL, Domaille DW, Chang CJ. Chem Rev. 2008; 108:1517–1549. [PubMed: 18426241]
19. Huang Z, Lippard SJ. Methods Enzymol. 2012; 505:445–468. [PubMed: 22289467]
20. Liu Z, He W, Guo Z. Chem Soc Rev. 2013; 42:1568–1600. [PubMed: 23334283]
21. Wong BA, Friedle S, Lippard SJ. J Am Chem Soc. 2009; 131:7142–7152. [PubMed: 19405465]
22. Koide Y, Urano Y, Hanaoka K, Terai T, Nagano T. ACS Chem Biol. 2011; 6:600–608. [PubMed: 21375253]
23. Frangioni JV. Curr Opin Chem Biol. 2003; 7:626–634. [PubMed: 14580568]
24. Hilderbrand SA, Weissleder R. Curr Opin Chem Biol. 2010; 14:71–79. [PubMed: 19879798]
25. Chan J, Dodani SC, Chang CJ. Nature Chem. 2012; 4:973–984. [PubMed: 23174976]
26. Yang Y, Zhao Q, Feng W, Li F. Chem Rev. 2013; 113:192–270. [PubMed: 22702347]
27. Minkin, VI. Molecular Switches. Feringa, BL.; Browne, WR., editors. Wiley-VCH Verlag GmbH & Co. KGaA; Weinheim: 2011.

28. Zhu JF, Yuan H, Chan WH, Lee AWM. Org Biomol Chem. 2010; 8:3957–3964. [PubMed: 20625584]
29. Zhu JF, Chan WH, Lee AWM. Tetrahedron Lett. 2012; 53:2001–2004.
30. Burdette SC, Walkup GK, Spingler B, Tsien RY, Lippard SJ. J Am Chem Soc. 2001; 123:7831–7841. [PubMed: 11493056]
31. Nolan EM, Lippard SJ. Acc Chem Res. 2009; 42:193–203. [PubMed: 18989940]
32. Zhang, X-a; Hayes, D.; Smith, SJ.; Friedle, S.; Lippard, SJ. J Am Chem Soc. 2008; 130:15788–15789. [PubMed: 18975868]
33. Lin W, Buccella D, Lippard SJ. J Am Chem Soc. 2013; 135:13512–13520. [PubMed: 23902285]
34. Qin Y, Miranda JG, Stoddard CI, Dean KM, Galati DF, Palmer AE. ACS Chem Biol. 2013; 8:2366–2371. [PubMed: 23992616]
35. Ueno Y, Jose J, Loudet A, Perez-Bolivar C, Anzenbacher P Jr, Burgess K. J Am Chem Soc. 2011; 133:51–55. [PubMed: 21105708]
36. Chirakul P, Hampton PD, Bencze Z. J Org Chem. 2000; 65:8297–8300. [PubMed: 11101388]
37. Bueno C, Villegas ML, Bertolotti SG, Previtali CM, Neumann MG, Encinas MV. Photochem Photobiol. 2002; 76:385–390. [PubMed: 12405144]
38. Vinkenborg JL, Nicolson TJ, Bellomo EA, Koay MS, Rutter GA, Merkx M. Nat Methods. 2009; 6:737–740. [PubMed: 19718032]
39. Neese F. WIREs Comput Mol Sci. 2012; 2:73–78.

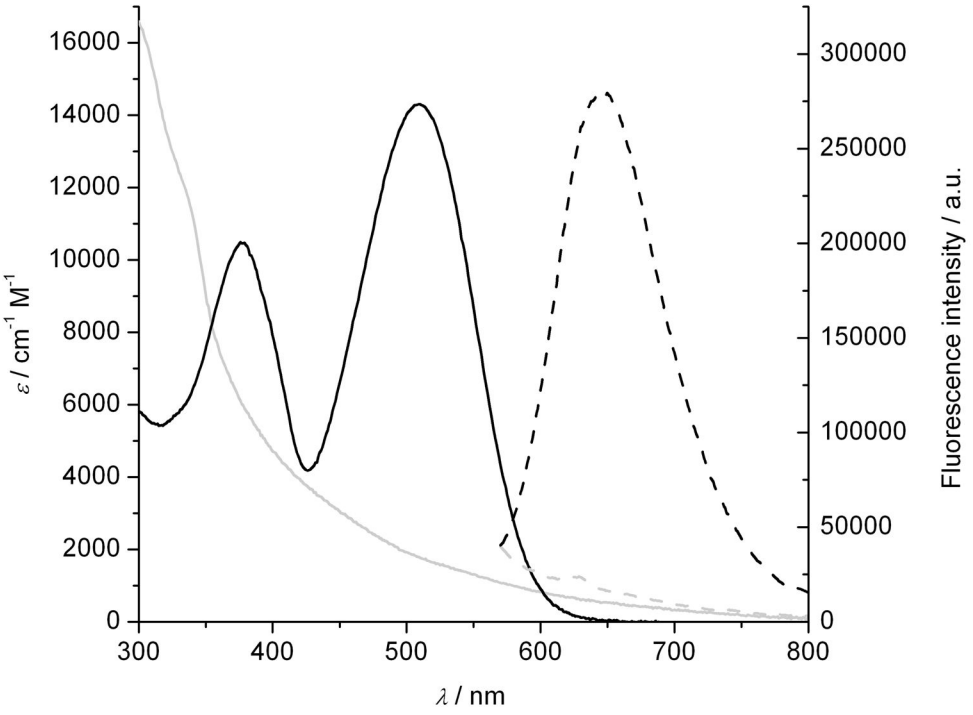

Figure 1.

Electronic absorption (solid lines) and fluorescence (dashed lines) spectra of SpiroZin1 before (grey lines) and after (black lines) addition of 10 equiv. of $ZnCl_2$. All measurements were performed using 5 μM SpiroZin1 in aqueous buffer (50 mM PIPES, 100 mM KCl, pH 7).

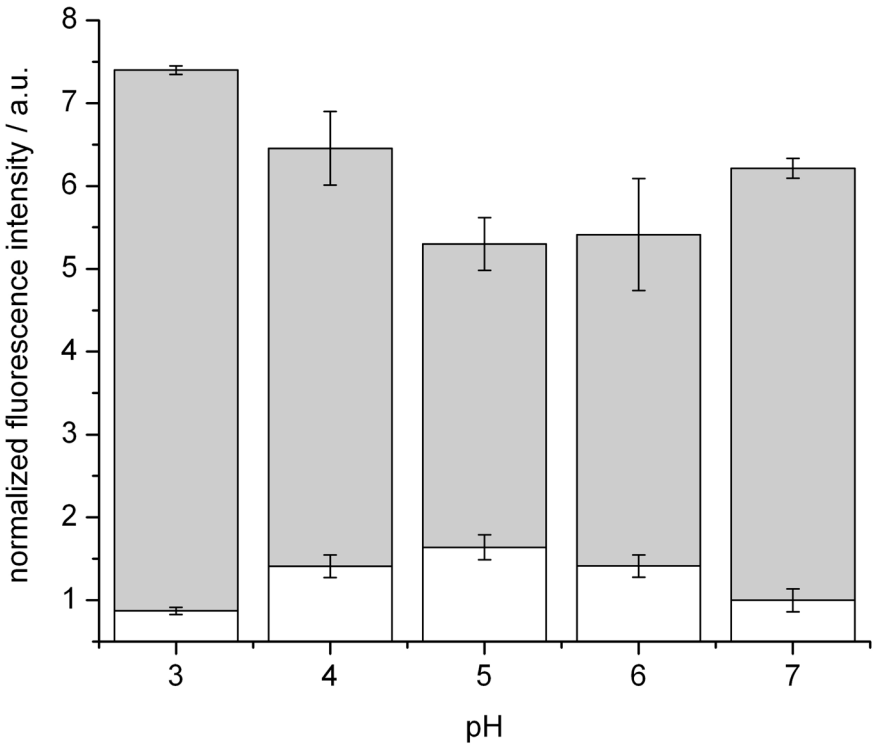

Figure 2.

Integrated fluorescence intensity of 5 μM SpiroZin1 at different pH values before (white bars) and after (grey bars) addition of 10 equiv. of $ZnCl_2$. The intensities were normalized with respect to 5 μM SpiroZin1 at pH 7 before addition of zinc.

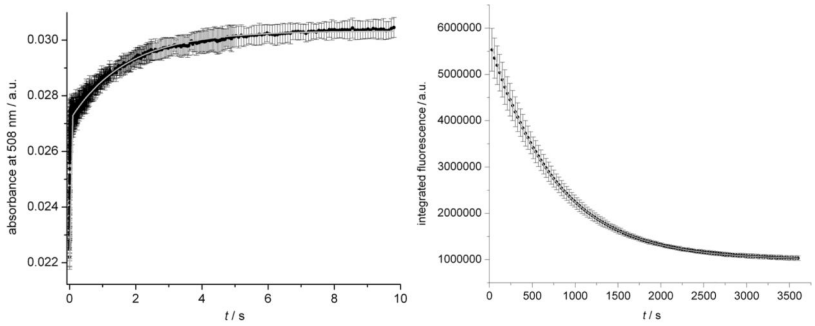

Figure 3.

Left: Increase in absorbance at 508 nm of 5 μM SpiroZin1 in aqueous buffer (50 mM PIPES, 100 mM KCl, pH 7) after addition of 100 equiv. of $ZnCl_2$. Right: Decrease in integrated fluorescence (550–800 nm, λ_{ex} = 508 nm) of 5 μM of zinc-bound SpiroZin1 in aqueous buffer (50 mM PIPES, 100 mM KCl, pH 7) after addition of 100 equiv. of EDTA.

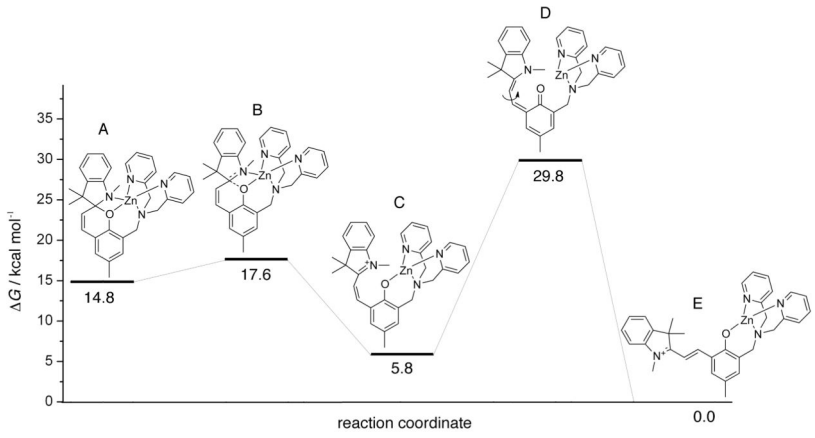

Figure 4.

Intrinsic reaction coordinate analysis of the zinc-induced, ring-opening reaction of SpiroZin1. A) Ring-closed starting structure; B) Ring-opening transition state; C) Open, cis cyanine intermediate; D) cis/trans isomerization transition state; E) Open, trans cyanine product.

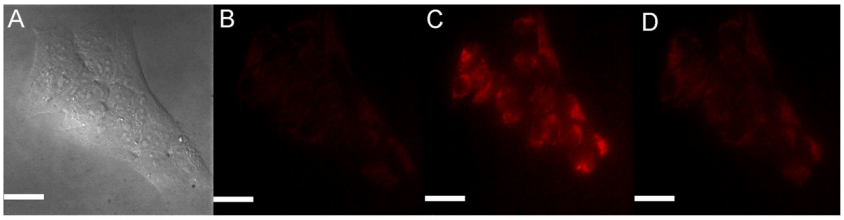

Figure 5.

Microscopy images of live HeLa cells incubated with 5 μM SpiroZin1. A) differential interference contrast (DIC) image; B) red channel image before addition of zinc pyrithione; C) red channel image after incubation with 20 μM zinc pyrithione; D) red channel image after incubating for 30 min with 50 μM TPEN. Scale bar = 25 μm. A color version of this figure can be found in the Supporting Information.

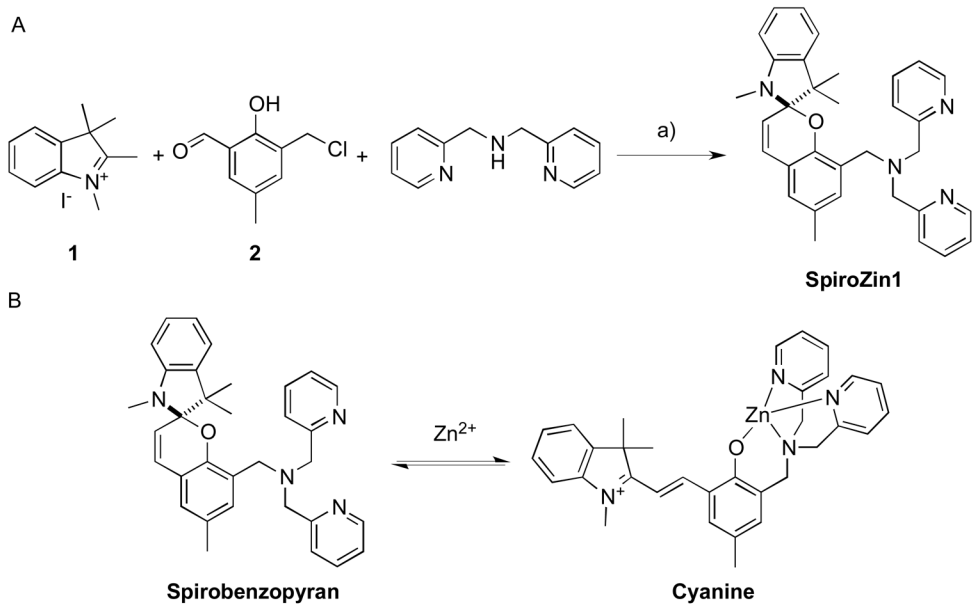

Scheme 1.

A) One-pot synthesis of SpiroZin1. Reactants and conditions: a) K_2CO_3, EtOH, reflux, 2 h, 40%. B) Reversible reaction of SpiroZin1 with Zn^{2+}.